

Bridging the hydrodynamic Drude model and local transformation optics theory

Rúben A. Alves ^{1,*}, Ariel Guerreiro,^{2,3,†} and Miguel Navarro-Cía ^{1,‡}

¹*School of Physics and Astronomy, University of Birmingham, Birmingham B15 2TT, United Kingdom*

²*Departamento de Física e Astronomia da Faculdade de Ciências da Universidade do Porto,*

Rua do Campo Alegre 687, 4169-007 Porto, Portugal

³*INESC TEC, Centre of Applied Photonics, Rua do Campo Alegre 687, 4169-007 Porto, Portugal*



(Received 10 January 2020; revised manuscript received 7 May 2020; accepted 8 May 2020; published 8 June 2020)

The recent ability of plasmonic nanostructures to probe subnanometer and even atomic scales demands theories that can account for the nonlocal dynamics of the electron gas. The hydrodynamic Drude model (HDM) captures much of the microscopic dynamics of the quantum mechanical effects when additional boundary conditions are considered. Here, we revisit the HDM under the Madelung formalism to reexpress its coupled system of equations as a single nonlinear Schrödinger equation in order to have a natural quantum mechanical description of plasmonics. Specifically, we study the response of two overlapping nanowires with this formalism. We ensure that an proposed frame concurs with classical electrodynamics when the local response approximation holds in the plasmonic system by finding the correction needed.

DOI: [10.1103/PhysRevB.101.235412](https://doi.org/10.1103/PhysRevB.101.235412)

I. INTRODUCTION

In the last decade, the advancements of nanofabrication techniques [1–3] and imaging [4,5] have allowed the field of plasmonics to expand at an exponential rate [6–14]. On the other hand, the theoretical framework needed to describe rigorously these plasmonic systems is still lacking. In fact, the classical Lorentz-Drude model still forms most of the theoretical background and modeling in use [15,16]. However, at the nanometric scale, the collective behavior of the conduction electrons is influenced by their quantum nature [17–20]. To describe these features, another model was introduced [21]. This model is called the hydrodynamic Drude model (HDM) as it describes the electrons in a metal as a charge fluid coupled with the electromagnetic field [22,23]. The main advantages of the HDM are that it takes into account atomic and subatomic interactions [22], in particular electron-electron repulsion, by considering the Pauli exclusion principle. The HDM has been used in numerical simulations of plasmonic nanostructures and has yielded a good agreement with the experimental data [24]. However, solving the fluid equations is not trivial as, for example, the geometry of the system is introduced by defining additional boundary conditions that can complicate the problem. To bypass this, we use the Madelung formalism [25].

The Madelung formalism was initially established to reexpress the Schrödinger equation in terms of the fluid equations that describe the flow of probability of the wave function in quantum systems [26]. The objective in this scenario is to proceed in the opposite direction, rewriting the fluid equations

in one nonlinear Schrödinger equation which can then be solved numerically. Unlike the standard HDM approaches found in the literature [24], our approach does not need to define the so-called additional boundary conditions to describe the geometry of the problem, as this is already defined with the linear terms of the potential in the Schrödinger equation.

The Madelung formalism allows us to describe a plasmonic system using the Schrödinger equation. Because of it, we can use methods commonly found in quantum mechanics and quantum optics to model our problem. Thus, pushing the analogy between plasmonic systems and atoms commonly discussed in the field: Plasmonic systems are often compared to meta-atoms since the collective behavior of the electrons in the metal can be discretized into modes much as an electron bound in the atom.

In this paper, we provide a linear analyses of this model by comparing the Rabi oscillations with the absorption cross section obtained by full-wave numerical calculations and transformation optics (TO) [27]. In order to do this comparison, we will simplify the HDM in association with the Madelung formalism to a linear equation with an abrupt interface between the metal and the dielectric.

II. PHYSICAL MODELS

A. Hydrodynamic Drude model

The HDM assumes that the motion of electrons in a metal (assumed nonmagnetic, $\mu_r = 1$) under the influence of an electromagnetic field are described by the fluid equations [28] that include the continuity equation,

$$-\partial_t n = \nabla \cdot (n\vec{u}), \quad (1)$$

and the Euler equation,

$$n\partial_t \vec{u} + n(\vec{u} \cdot \nabla)\vec{u} = -\frac{ne}{m_e}(\vec{E} + \vec{u} \times \vec{B}) - \frac{\nabla P}{m_e} - \gamma n\vec{u}, \quad (2)$$

*rx721@bham.ac.uk

†asguerre@fc.up.pt

‡m.navarro-cia@bham.ac.uk

where n , \vec{u} , m_e , and e are the electron density, velocity, mass, and charge, respectively, and \vec{E} and \vec{B} are the electric and magnetic fields of the electromagnetic radiation, respectively. In Eq. (2), $e(\vec{E} + \vec{u} \times \vec{B})$ represents the Lorentz force, ∇P describes the Thomas-Fermi pressure (a pressure that accounts for the Pauli exclusion principle), and $\gamma \vec{u}$ represents the damping forces (a phenomenological parameter that accounts for the damping due to electron-ion collisions).

To apply the Madelung formalism, one starts with the Schrödinger equation

$$i\hbar\alpha\partial_t\psi = \left[-\frac{\hbar^2\beta}{2m_e}\nabla^2 + V \right]\psi, \quad (3)$$

where α and β are normalizing constants. In order to transform Eq. (3) into Eqs. (1) and (2), we assume that the solution to this Schrödinger equation takes the form of $\psi = n^{1/2}e^{iS}$. Replacing this in Eq. (3) and separating it in two equations, one with the real part and the other with the imaginary part, yields

$$-\hbar\alpha\dot{S} = -\frac{\hbar^2\beta}{2m_e}\left[\frac{1}{2}\frac{\nabla^2 n}{n} - \frac{1}{4}\left(\frac{\nabla n}{n}\right)^2 - (\nabla S)^2 \right] + V \quad (4)$$

for the real part, and

$$\frac{\hbar\alpha}{2}\dot{n} = \left[-\frac{\hbar^2\beta}{2m_e}\left(\nabla^2 S + \frac{\nabla n \nabla S}{n}\right) \right]n \quad (5)$$

for the imaginary part.

If one now assumes that the magnetic component of an electromagnetic wave is so small that it can be neglected when compared to its electric counterpart, it is possible to define $\nabla S = u$. Hence Eq. (4) is reduced to

$$\dot{n} = -\frac{\beta}{\alpha}\frac{\hbar}{m_e}\nabla \cdot (nu). \quad (6)$$

Comparing Eq. (6) with Eq. (1) yields

$$\frac{\beta}{\alpha}\frac{\hbar}{m_e} = 1. \quad (7)$$

From Eq. (5), one has

$$-\dot{S} = -\frac{\beta}{\alpha}\frac{\hbar}{2m_e}\left[\frac{1}{2}\frac{\nabla^2 n}{n} - \frac{1}{4}\left(\frac{\nabla n}{n}\right)^2 - (\nabla S)^2 \right] + \frac{1}{\alpha\hbar}V, \quad (8)$$

defining $V = V' - \beta V_B$, where

$$V_B = -\frac{\hbar^2}{4m}\left[\frac{\nabla^2 n}{n} - \frac{1}{2}\left(\frac{\nabla n}{n}\right)^2 \right] = -\frac{\hbar^2}{4m_e}\frac{\nabla^2\sqrt{n}}{\sqrt{n}} \quad (9)$$

is the Bohm potential. With this in mind, and recalling that $\nabla S = u$, Eq. (8) simplifies to

$$-\dot{u} = \frac{\beta}{\alpha}\frac{\hbar}{2m_e}\nabla(u \cdot u) + \frac{1}{\alpha\hbar}\nabla V'. \quad (10)$$

Rearranging Eq. (10), one has

$$n\dot{\vec{u}} + n(\vec{u} \cdot \nabla)\vec{u} = -\frac{m_e}{\beta\hbar^2}n\nabla V'. \quad (11)$$

Comparing this equation to the original fluid equation, one concludes that

$$\nabla V' = \frac{\beta\hbar^2 e}{m_e^2}\vec{E} + \frac{\beta\hbar^2}{m_e^2}\frac{1}{n}\nabla P + \gamma\frac{\beta\hbar^2}{m_e}\vec{u} + \frac{\beta\hbar^2}{m_e^2}\nabla\mathcal{U}, \quad (12)$$

where \vec{E} is the electric field, ∇P is the Thomas-Fermi pressure, γ the losses coefficient, and \mathcal{U} the confining potential. As the magnetic component of an electromagnetic wave is small when compared to its electric counterpart and assuming a perfect metal with no losses, the potential takes the form of

$$V = \frac{\beta\hbar^2 e}{m_e^2}\vec{r} \cdot \vec{E} + \frac{\beta\hbar^2}{m_e^2}\frac{(3\pi^2)^{2/3}h^2}{2m_e}n^{2/3} + \frac{\beta\hbar^2}{m_e^2}\mathcal{U} + \beta\frac{\hbar^2}{4m_e}\frac{\nabla^2\sqrt{n}}{\sqrt{n}}. \quad (13)$$

The definition $\psi = n^{1/2}e^{iS}$ implies that $n = n_0|\psi|^2$, which means that the full potential on the Schrödinger equation takes the form

$$V = \frac{\beta\hbar^2 e}{m_e^2}\vec{r} \cdot \vec{E} + \frac{\beta\hbar^2}{m_e^2}\frac{(3\pi^2)^{2/3}h^2 n_0^{2/3}}{2m_e}|\psi|^{4/3} + \frac{\beta\hbar^2 e}{m_e^2}\mathcal{U}[eV] + \beta\frac{\hbar^2}{4m_e}\frac{\nabla^2\sqrt{|\psi|^2}}{\sqrt{|\psi|^2}}. \quad (14)$$

Equation (14) shows the full potential that arises in transforming the fluid equations into a single Schrödinger equation. One could argue that, because it is a nonlinear equation, it is as cumbersome to solve as the actual fluid equations. Yet one could use the Madelung formalism and then simplify the model by only considering the linear contributions of the potential and then step by step introducing the nonlinear terms.

After defining the Schrödinger equation, the analogy between plasmonic systems and problems found in quantum mechanics has been established. Thus, one can use methods commonly found in quantum mechanics such as the Rabi oscillations, which we describe succinctly next. A full derivation of the Rabi oscillations can be found in Appendix A, though.

Assuming that the field is tuned to the transition of two plasmonic modes, the wave function can be written as

$$\psi = C_a\varphi_a + C_b\varphi_b, \quad (15)$$

so Eq. (3) transforms into

$$\partial_t \begin{bmatrix} C_a \\ C_b \end{bmatrix} = -i \begin{bmatrix} \Omega_{AA}(t) & \Omega_{AB}(t) \\ \Omega_{BA}(t) & \Omega_{BB}(t) \end{bmatrix} \begin{bmatrix} C_a \\ C_b \end{bmatrix}. \quad (16)$$

Equation (16) is analogous to the Bloch equations derived from the interaction of a two-level atom with a resonant or near-resonant electromagnetic field. In the interaction picture, Eq. (16) changes to

$$\partial_t \begin{bmatrix} C_a \\ C_b \end{bmatrix} = -i \begin{bmatrix} 0 & \Omega(t) \\ \Omega^*(t) & 0 \end{bmatrix} \begin{bmatrix} C_a \\ C_b \end{bmatrix}, \quad (17)$$

with $\Omega(t) \equiv \Omega_{A,B}$.

Assuming the rotating-wave approximation, one arrives at

$$|C_b(t)|^2 = \frac{\Omega^2}{\Omega'^2} \sin^2\left(\frac{\Omega't}{2}\right), \quad (18)$$

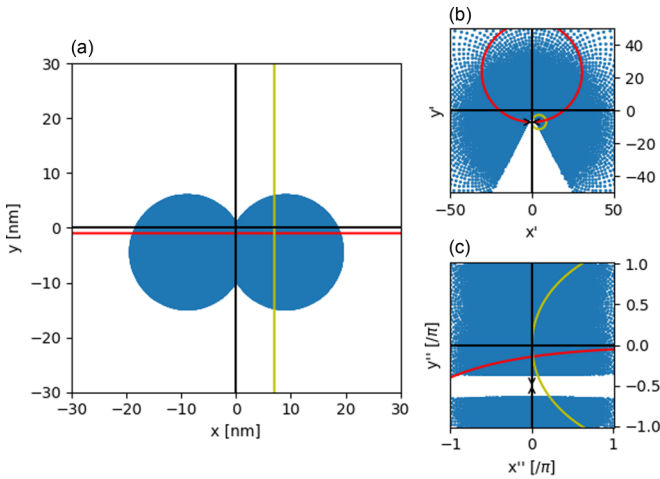


FIG. 1. (a) Cross section of the proposed plasmonic system to be studied. (b) Cross section of the proposed plasmonic system after the first transformation. (c) Cross section of the system after the second transformation. The yellow and red lines are visual aids of the transformations.

where $\Omega' = \sqrt{\Omega^2 + \Delta^2}$, with Δ as the detuning and $\Omega = \langle A | H_I | B \rangle$ where A and B are the two energy levels. Equation (18) represents the probability of an electromagnetic wave, with frequency ω , to excite the system from the state $|A\rangle$ to the state $|B\rangle$ by absorbing a photon. The amplitude of this probability [and not the energy levels calculated from Eq. (3)] is closely related to a macroscopic property of the system called the absorption cross section [5] that can be obtained from full-wave simulations and TO.

The above derivation is a general one. From now on, we will apply it to a specific plasmonic system assuming an infinite potential: two overlapping nanowires [see Fig. 1(a)]. We choose this system because we can solve it analytically using TO as outlined next and we can further validate the results with full-wave simulations. The metal properties for the TO and the full-wave simulations are described in Appendix B.

B. Transformation optics

Another analytical method gaining momentum to describe plasmonic systems is TO and its two-dimensional (2D) variant known as conformal transformation [27,29]. These techniques transpose a complex plasmonic system to a simpler system, whereby it would be easier to solve analytically; then the solution of the original problem is calculated by using the inverse transformation. Under such transformations, Maxwell's equations are invariant. In the last few years, this method has gained quite a bit of popularity as it allows the description of a wide range of plasmonic systems [7,29–36].

In the 2D case as the one chosen in this paper, conformal transformations are special coordinate transformations that preserve orientation and angles locally [27,29]. Hence, the tangential component of the electric field and the normal component of the displacement field are conserved, too. As such, the material in the real and virtual world are identical. For that local angle orientation preservation, the transformation needs to satisfy the Cauchy-Riemann relations [34] that are given

by $\frac{\partial x}{\partial x'} = \frac{\partial y}{\partial y'}$ and $\frac{\partial x}{\partial y'} = -\frac{\partial y}{\partial x'}$, where (x, y) is the coordinate system of the real world and (x', y') of the virtual world.

In order to describe our overlapping nanowires with TO, we define $z = x + iy$, where x and y are the coordinates of the real world and apply two transformations [36,37]. The first transformation is

$$z' = \frac{g^2}{z} - ir_0, \quad (19)$$

where r_0 is a constant that relates to the intensity of the electromagnetic field in the real world and the position of the dipole in the first virtual world, $z' = x' + iy'$ are the coordinates of the first virtual world, and $g^2 = 2r_0\sqrt{R^2 - \frac{D^2}{4}}$, where R is the radius of a single nanowire and D is the distance between the two centers of each nanowire.

The second transformation follows

$$z'' = \ln\left(\frac{z'}{r_0}\right), \quad (20)$$

where $z'' = x'' + iy''$ are the coordinates of the second virtual world. The resulting geometry after each transformation can be seen in Figs. 1(b) and 1(c).

If the original two overlapping nanowires are illuminated by a plane wave, such a plane wave is transformed into an array of x'' - or y'' -polarized dipoles depending if the plane wave is y or x polarized, respectively. In this paper, we consider an x -polarized plane wave only to excite the fundamental plasmon modes.

Given the subwavelength size of the plasmonic system considered, the problem can be treated quasistatically. Thus, the electric field is completely described by an electrostatic potential and such an electrostatic potential is conserved after the conformal mapping due to its holomorphic nature. Hence, the underlying physics of the two overlapping wires can be found by solving the potential in one period of the infinite periodic metal-dielectric system [36,37]. The solution starts by finding the potential generated by the dipole in such a period, which involves calculating its corresponding expansion coefficient $a(k)$. Then, a set of three equations is defined that describes the total potential in the dielectric region above and below the dipole, and in the metal region. The expansion coefficients associated with the scattering potential in the dielectric $b(k)$ and metal region $c(k)$ are determined by applying boundary conditions: the conservation of the tangential electric field and the normal displacement field.

From the tangential electric field one has

$$a(k)e^{-k\theta_0} + b(k)(e^{-k\theta_0} - e^{k\theta_0}) = c(k)(e^{-k\theta_0} - e^{-k(2\pi - \theta_0)}), \quad (21)$$

and from the normal displacement field

$$a(k)e^{-k\theta_0} + b(k)(e^{-k\theta_0} + e^{k\theta_0}) = \varepsilon c(k)(e^{-k\theta_0} + e^{-k(2\pi - \theta_0)}), \quad (22)$$

where $2\theta_0$ is the distance between two consecutive metal slabs, in the second virtual world.

Once $b(k)$ and $c(k)$ are found, the dispersion relation is derived by imposing that these scattering coefficients diverge, yielding

$$\varepsilon \tanh(k\theta_0) = -\tanh[k(\pi - \theta_0)]. \quad (23)$$

The complete derivation of Eq. (23) can be seen in Appendix C. By solving Eq. (23), one can find the relationship between ω and k . With this relationship and recalling that the electric field is the gradient of the electric potential, one can now deduce the electric field at the dipole position as

$$\vec{E}(z'' = iy_n'') = -i \frac{\Theta}{2\epsilon\theta_0} \Gamma k, \quad (24)$$

where y_n is the position of the n th dipole, Θ is the amplitude of the dipole, and Γ is defined as

$$\Gamma = \frac{\epsilon \cosh^{-1}(k\theta_0) e^{-k\theta_0} [1 + \tanh(k\theta_0)]}{\epsilon - \epsilon_c + \epsilon(\epsilon\epsilon_c - 1) \tanh^2(k\theta_0)}, \quad (25)$$

where $\epsilon_c = \frac{\theta_0 - \pi}{\theta_0}$.

The power dissipated in the virtual world is given by

$$P_a = -\frac{\omega}{2} \text{Im}\{\Theta^* e_x \cdot \vec{E}(z'' = iy_n'')\}, \quad (26)$$

where Im stands for the imaginary part and is identical to the power dissipated in the real world because of the quasistatic treatment and the properties of conformal transformation. Hence, the absorption cross section of our system can then be calculated with

$$\sigma_a = \frac{P_a}{P_{\text{in}}} = 2\pi^2 k_0 \frac{\Sigma^2}{\theta_0} \text{Re}\{k\Gamma\}, \quad (27)$$

where P_{in} is the intensity of the plane wave, $\Sigma = D \sin(\theta_0)$, k_0 is the wave vector in vacuum, and Re stands for the real part.

III. RESULTS AND DISCUSSION

In order to test the models presented here, we have chosen to describe a plasmonic system comprising two overlapping nanowires. The cross section of a system such as that can be compared to a diatomic molecule when the Madelung formalism is used and this will be discussed first. The system can also be analyzed analytically with the assistance of conformal transformation [37] (see Fig. 1 for the cascaded conformal transformations to arrive at a canonical infinite periodic metal-dielectric system) and the results following this methodology will be discussed afterwards and compared against the Madelung formalism approach. However, in order to do this comparison we have to simplify the model to its local limit. This can be achieved by linearizing the Schrödinger equation and by defining the linear potential with a sharp interface between the metal and the surrounding environment.

To describe this system using the Madelung formalism, one needs to first find the solutions of the linear coefficients of the Schrödinger equation [Eq. (3), with the term V being the linear parts of Eq. (14)], where the term \mathcal{U} is defined to force the electron density profile to abruptly vanish at the metal interface. These solutions to the linear Schrödinger equation can be seen in Fig. 2 for a distance between the centers of each nanowire of $D = 16$ nm. Notice that these electron density distributions do not represent directly the plasmonic modes of the nanostructure. These solutions were found using the finite-difference method that is described in more detail in Appendix D. As expected, each solution can be defined by the number of nodes inside the potential well and the probability of finding an electron in the position z varies for each state.

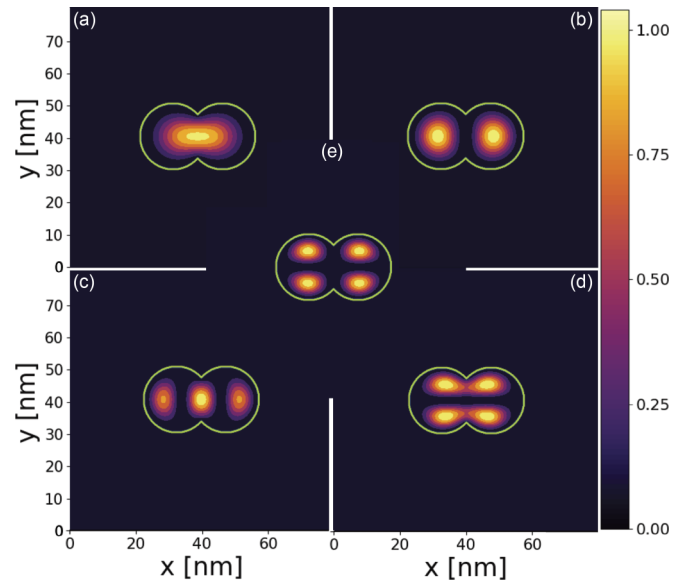


FIG. 2. Normalized electron density distribution for the (a) first, (b) second, (c) third, (d) fourth, and (e) fifth plasmonic energy levels of two overlapping nanowires with $R = 10$ nm and $D = 15$ nm.

A full parametric study was done and the evolution of the energy levels for each D can be seen in Fig. 3. With these results, one can now make use of the Rabi oscillations, commonly used in quantum optics, to calculate the probability of a change in the state of the plasmon mode of the nanostructure. In practice, the plasmonic structure acts as a small antenna which absorbs and reemits light. Given the total size of the overlapping nanowires, scattering can be neglected. Thus, the absorption of light is proportional to $|C_b(t)|^2$ from Eq. (18) in a two-level system. It is important to note that as one increases the distance D closer to 20 nm, the modes start to trend back to their original position with extra degeneracy. This is because in the limit, instead of having two overlapping nanowires, we

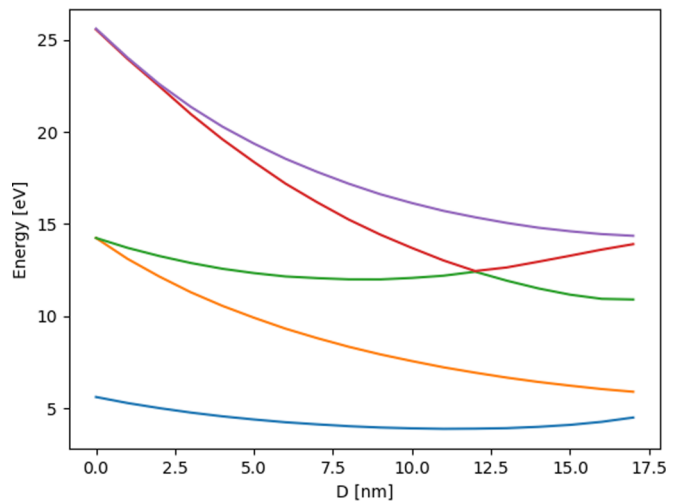


FIG. 3. First five energy levels for two overlapping circular nanowires of $R = 10$ nm as a function of the distance D , calculated from using the inverted Madelung formalism after linearization of the potential.

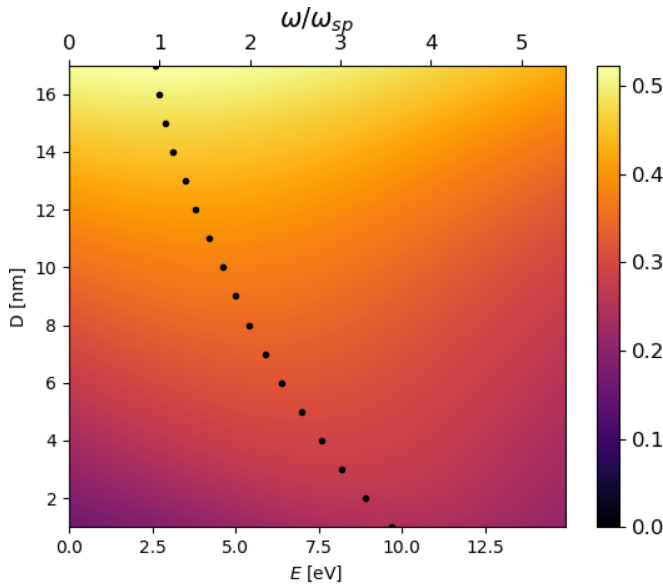


FIG. 4. Linear combination for all the Rabi coefficients for a five-level system and where the dots represent the maximum. Notice that the energy depicted is the energy of light.

have two isolated nanowires. Another feature in Fig. 3 is the crossing of the third and fourth mode at around $D = 12$ nm. This happens because, as D increases, the shift of energy of these two modes [Figs. 2(c) and 2(d)] is so large that they actually trade places when sorting them by their value of energy.

In Fig. 4 one can see the linear combination of all the Rabi coefficients for a five-level system and their relationship with the distance D and the energy of light defined both in eV and ω/ω_{sp} , where ω_{sp} is the surface plasmon frequency. This is done by using Eq. (17) for every combination possible between the five-level system considered. It is important to note that the solution used in the Madelung formalism is a linear combination of all of the eigenstates. Since it is impossible to compute all of these states, as there is an infinite amount of them (for an infinite potential there is an infinite amount of eigenstates), we restrict ourselves to the first five as it gives a clear enough physical picture. These results can now be compared to the ones obtained using TO.

Equation (23) is a transcendental equation, so the solutions to Eq. (27) were found using a PYTHON code and can be seen in Fig. 5. Even though TO has been widely confirmed in the field, we have compared its solutions to a full-wave solution using COMSOL, which can be seen in Fig. 6. The scattering cross section was also computed using COMSOL (not shown) to confirm that it is negligible. By comparing Fig. 5 with Fig. 6, one can see that the first mode from the COMSOL simulation matches directly with the one obtained using TO. We refer the reader to Appendix E to see the field distribution and charge density of this first mode along with the first higher-order mode. One should note as well that by using the TO formulation, higher-order modes are not captured when a plane wave is the excitation, but the model is able to do it when the plasmonic system is pumped by a nearby nanoemitter [29,30,35,38].

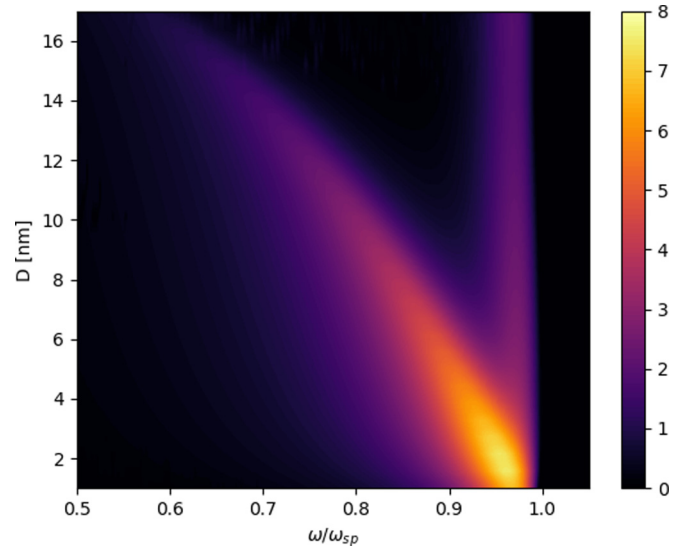


FIG. 5. Absorption cross section for two circular overlapping nanowires of $R = 10$ nm as a function of the distance between their centers D using TO. Notice that it is normalized to the system's length along the dimer axis.

Figure 7 shows the ratio of the energy of the absorption cross-section maximum obtained with TO and the energy of the maximum of the Rabi oscillations (maximum probability of absorbing a photon that results into a state transition) obtained with the HDM with the Madelung formalism for each value of D . For largely overlapping nanowires, higher-order modes emerge close to the fundamental mode, influencing greatly the latter. For less overlapping nanowires (i.e., larger values of D), even though there are more higher-order modes to be considered, their influence on the fundamental mode decreased as it is redshifted significantly with respect to the higher-order modes. Hence, the ratio shown in Fig. 7

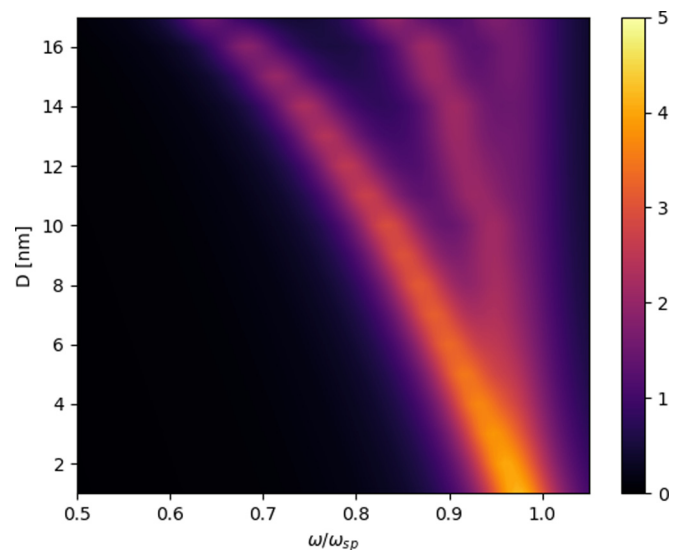


FIG. 6. Absorption cross section for two circular overlapping nanowires of $R = 10$ nm as a function of the distance between their centers D using full-wave COMSOL simulations. Notice that it is normalized to the system's length along the dimer axis.

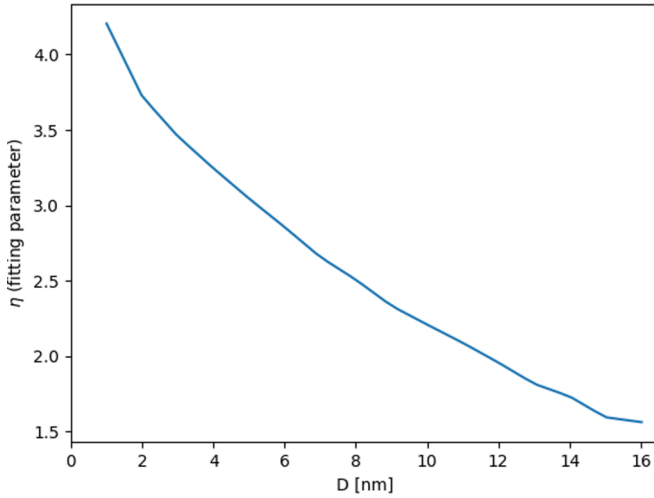


FIG. 7. Comparison between TO and the HDM with the Madelung formalism as a function of D .

decreases as a function of D . In addition, the effects of nonlocality are known to decrease for larger structures, making the results of the Madelung formalism and HDM more comparable to the local TO. The fact that this ratio is not linear means that only solving the linear potentials of the Schrödinger equation does not completely result in the local limit of the HDM. Hence, the linearized Madelung formalism still partially retains nonlocality.

IV. CONCLUSIONS

In this paper, we described the initial steps toward an original complete theoretical framework for the so-called classical (macroscopic) to quantum (microscopic) boundary, from a quantum viewpoint rather than the classical viewpoint as done rigorously by others recently [20]. In particular, we presented another way to look at the hydrodynamic Drude model for plasmonics using the Madelung formalism in order to rewrite the fluid equations into a Schrödinger equation. For the total population plasmonic system in the steady state to be tractable (because of computational constraint), we restricted ourselves to the five fundamental energy levels. This method allowed us to describe the behavior of the fundamental localized surface plasmon mode in the two overlapping nanowire plasmonic systems under the local limit and assuming a classical, macroscopic sharp dielectric-metal boundary. Notice that defining a linear potential with a nonsharp boundary to account for electron spill-out is possible in our model and will be addressed elsewhere. We then compared the results with the ones obtained using transformation optics to find the necessary correction to the model to account for the effective potential. With such a semiempirical correction that ensures that our model is valid in the local limit, one can start tackling the nonlinear terms of the Schrödinger equation, and thus incorporating in a natural way nonlocality without the need for defining additional boundary conditions, which is the current approach in plasmonics and is highly contested.

ACKNOWLEDGMENTS

We wish to acknowledge the help provided by Dr. N. A. Silva for his valuable and constructive suggestions during the initial development of this work. R.A.A. is supported by the University of Birmingham (Ph.D. studentship). M.N.-C. is supported by the University of Birmingham (Birmingham Fellowship).

APPENDIX A: RABI OSCILLATIONS

Assume that the system can be described by a two-level system, $|g\rangle$ (for the ground state) with energy $\hbar\omega_g$ and $|e\rangle$ (for the excited state) with energy $\hbar\omega_e$. The Hamiltonian for the coupling of this system and a radiation field of frequency ω can be written as follows,

$$H = H_0 + H_I, \quad (\text{A1})$$

where H_I is called the interaction Hamiltonian defined by $H_I = r \cdot E_0 \cos(\omega t)$, and H_0 represents the unperturbed system. The solution to the Schrödinger equation of the unperturbed system can be written as

$$\psi(r, t) = c_g(t) |g\rangle e^{-i\omega_g t} + c_e(t) |e\rangle e^{-i\omega_e t}. \quad (\text{A2})$$

Applying Eq. (A2) in Eq. (A1) yields

$$\begin{aligned} i\hbar\partial_t [c_g(t) |g\rangle e^{-i\omega_g t} + c_e(t) |e\rangle e^{-i\omega_e t}] \\ = H(t) [c_g(t) |g\rangle e^{-i\omega_g t} + c_e(t) |e\rangle e^{-i\omega_e t}], \end{aligned} \quad (\text{A3})$$

and expanding and simplifying this turns into

$$\begin{aligned} i\hbar\partial_t c_g e^{-i\omega_g t} |g\rangle + i\hbar\partial_t c_e e^{-i\omega_e t} |e\rangle \\ = H_I e^{-i\omega_g t} c_g |g\rangle + H_I e^{-i\omega_e t} c_e |e\rangle. \end{aligned} \quad (\text{A4})$$

Applying $\langle g|$ and $\langle e|$ to Eq. (A4) we have

$$i\hbar\partial_t c_g = c_g \langle g| H_I |g\rangle + e^{-i(\omega_e - \omega_g)t} c_e \langle g| H_I |e\rangle, \quad (\text{A5})$$

and

$$i\hbar\partial_t c_e = e^{-i(\omega_e - \omega_g)t} c_g \langle e| H_I |g\rangle + c_e \langle e| H_I |e\rangle. \quad (\text{A6})$$

Notice that in doing so we are computing the energy levels of the dressed states (the eigenstates of the system composed of plasmons and light) by opposition to the undressed states, which refer to eigenstates of the plasmons considering only the confinement potential produced by the metal geometry.

To simplify this notation, let us define

$$\Omega_{ij} = \hbar^{-1} \langle i| H_I |j\rangle e^{-i(\omega_j - \omega_i)t}. \quad (\text{A7})$$

With this notation, Eqs. (A5) and (A6) can be written as

$$\partial_t \begin{bmatrix} c_g \\ c_e \end{bmatrix} = -i \begin{bmatrix} \Omega_{AA}(t) & \Omega_{AB}(t) \\ \Omega_{BA}(t) & \Omega_{BB}(t) \end{bmatrix} \begin{bmatrix} c_g \\ c_e \end{bmatrix}, \quad (\text{A8})$$

and in the interaction picture, it changes to

$$\partial_t \begin{bmatrix} c_g \\ c_e \end{bmatrix} = -i \begin{bmatrix} 0 & \Omega(t) \\ \Omega^*(t) & 0 \end{bmatrix} \begin{bmatrix} c_g \\ c_e \end{bmatrix}, \quad (\text{A9})$$

with $\Omega(t) \equiv \Omega_{ge}$. If we now apply the rotating-wave approximation (for this approximation, we assume that the electric

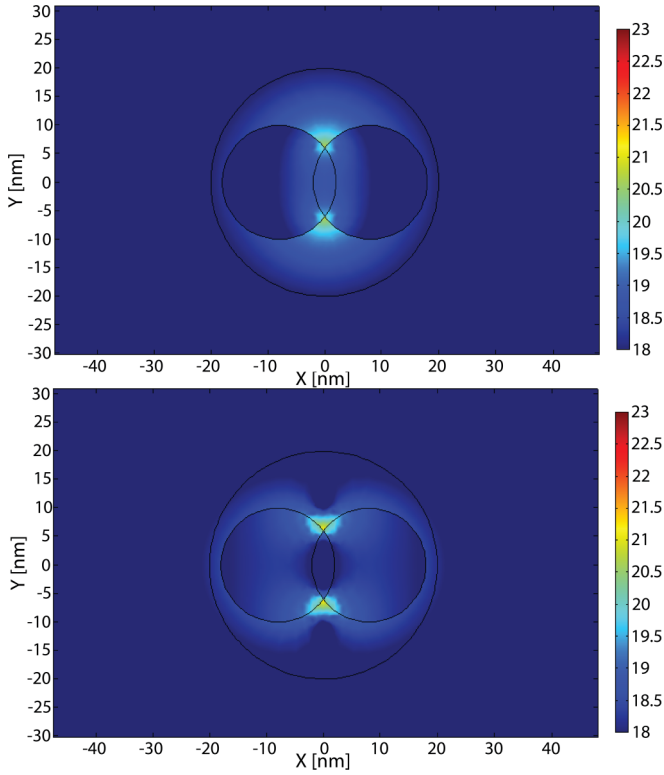


FIG. 8. Spatial intensity distribution in logarithm scale of the first (top) and second (bottom) plasmonic modes of the two overlapping nanowires found using COMSOL full-wave simulations.

field period is much faster than the response of the atom), one arrives at

$$|c_e(t)|^2 = \frac{\Omega^2}{\Omega'^2} \sin^2\left(\frac{\Omega't}{2}\right), \quad (\text{A10})$$

where $\Omega' = \sqrt{\Omega^2 + \Delta^2}$.

With Eq. (A10), we can relate the amplitude of this probability to the macroscopic property of the system that is the absorption cross section.

APPENDIX B: METAL MODEL

Both the TO and the full-wave simulations considered the same ideal metal whose concentration of free electrons per unit volume is 1.07×10^{28} , and thus has the following dielectric permittivity,

$$\varepsilon = 1 - \frac{\omega_p^2}{\omega^2 + i\gamma\omega}, \quad (\text{B1})$$

where $\omega_p = 5.8353 \times 10^{15}$ rad/s, $\gamma = 2.861364884 \times 10^{14}$ rad/s.

APPENDIX C: CHARACTERISTIC EQUATION FROM THE TRANSFORMATION OPTICS METHOD

In order to arrive at the dispersion relation of the system considered, one has to rearrange Eqs. (21) and (22). So from Eq. (21), one has

$$\begin{aligned} a(k)e^{-k\theta_0} + b(k)(e^{-k\theta_0} - e^{k\theta_0}) \\ = c(k)e^{-k\pi}(e^{k(\pi-\theta_0)} - e^{-k(\pi-\theta_0)}), \end{aligned} \quad (\text{C1})$$

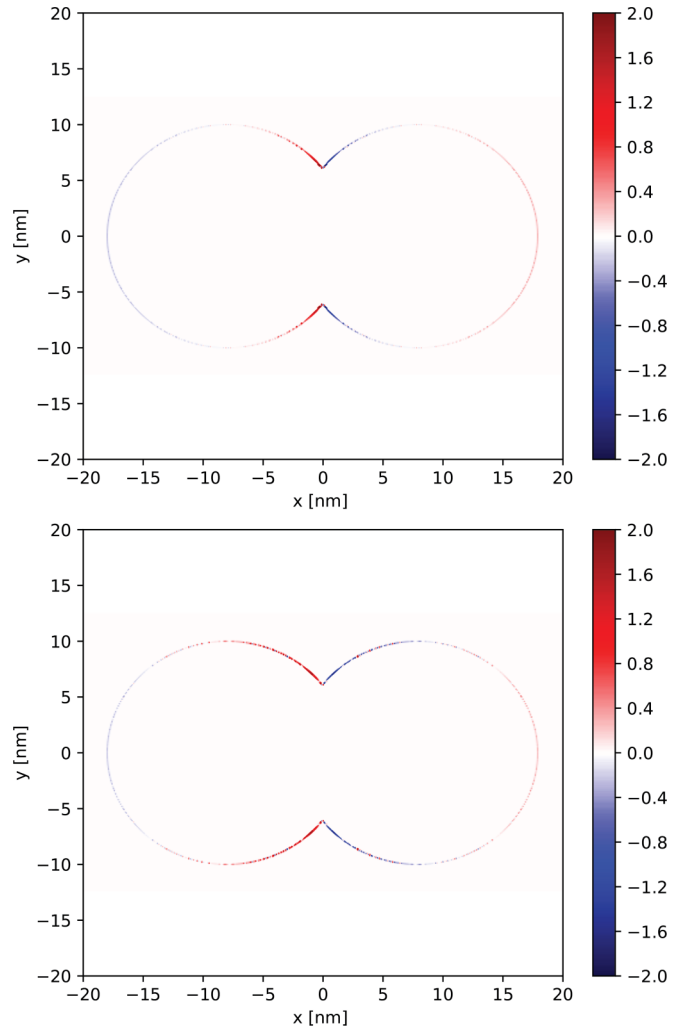


FIG. 9. Numerically computed charge density of the first (top) and second (bottom) plasmonic modes of the two overlapping nanowires. The scale color bars are saturated to better appreciate the charge density.

and from Eq. (22),

$$\begin{aligned} a(k)e^{-k\theta_0} + b(k)(e^{-k\theta_0} + e^{k\theta_0}) \\ = \varepsilon c(k)e^{-k\pi}(e^{k(\pi-\theta_0)} + e^{-k(\pi-\theta_0)}). \end{aligned} \quad (\text{C2})$$

Dividing Eq. (C1) with Eq. (C2) yields

$$\frac{a(k)e^{-k\theta_0} + b(k)(e^{-k\theta_0} - e^{k\theta_0})}{\varepsilon \frac{a(k)e^{-k\theta_0} + b(k)(e^{-k\theta_0} + e^{k\theta_0})}{\varepsilon}} = \tanh[k(\pi - \theta_0)]. \quad (\text{C3})$$

Organizing Eq. (C3), one has

$$b(k) = \frac{a(k)e^{-k\theta_0}}{2} \frac{\varepsilon - \tanh[k(\pi - \theta_0)]}{\cosh(k\theta_0)\{\varepsilon \tanh(k\theta_0) + \tanh[k(\pi - \theta_0)]\}}. \quad (\text{C4})$$

Replacing Eq. (C4) in Eq. (C1), one can find the definition of $c(k)$ to be

$$\begin{aligned} c(k) = \frac{a(k)}{2} \frac{e^{k\pi} e^{-k\theta_0}}{\cosh[k(\pi - \theta_0)]} \\ \times \varepsilon \frac{\tanh(k\theta_0) + 1}{\varepsilon \tanh(k\theta_0) + \tanh[k(\pi - \theta_0)]}, \end{aligned} \quad (\text{C5})$$

which simplifies to

$$c(k) = \frac{a(k)}{2} \frac{\varepsilon e^{k\pi}}{\cosh(k\theta_0) \cosh[k(\pi - \theta_0)]} \times \frac{1}{\varepsilon \tanh(k\theta_0) + \tanh[k(\pi - \theta_0)]}. \quad (\text{C6})$$

The characteristic equation can then be found when both $b(k)$ and $c(k)$ diverge. That happens when

$$\varepsilon \tanh(k\theta_0) = -\tanh[k(\pi - \theta_0)]. \quad (\text{C7})$$

APPENDIX D: FINITE-DIFFERENCE METHOD

The Hamiltonian for the linear components of the Schrödinger equation were defined using the finite-difference method and sparse matrices. This method works by approx-

imating a derivative with an equation of differences [39]. A sparse matrix is a matrix that contains mostly zeros. In order to save memory, in numerical methods that use a sparse matrix, the computer only stores the nonzero elements and their position.

APPENDIX E: ELECTRIC FIELD AND CHARGE DENSITY

Figure 8 shows the spatial intensity distribution of the first two plasmonic modes in the two overlapping nanowire plasmonic system with $R = 10$ nm and $D = 16$ nm. The corresponding frequencies are $\omega = 0.685\omega_{\text{sp}}$ and $0.877\omega_{\text{sp}}$, respectively. For both modes, the field is extremely confined and intense in the vicinity of the structure singularities, that is, the points where the two nanowires merge.

Figure 9 shows the charge density for the first two plasmonic modes in the two overlapping nanowire plasmonic system with $R = 10$ nm and $D = 16$ nm.

-
- [1] H. Shao, H. Im, C. M. Castro, X. Breakefield, R. Weissleder, and H. Lee, *Chem. Rev.* **118**, 1917 (2018).
- [2] A. Corma, J. Navas, and M. J. Sabater, *Chem. Rev.* **118**, 1410 (2018).
- [3] N. C. Lindquist, P. Nagpal, K. M. McPeak, D. J. Norris, and S.-H. Oh, *Rep. Prog. Phys.* **75**, 036501 (2012).
- [4] G. X. Ni, A. S. McLeod, Z. Sun, L. Wang, L. Xiong, K. W. Post, S. S. Sunku, B. Y. Jiang, J. Hone, C. R. Dean, M. M. Fogler, and D. N. Basov, *Nature (London)* **557**, 530 (2018).
- [5] L. Novotny and B. Hecht, *Principles of Nano-Optics* (Cambridge University Press, Cambridge, 2006).
- [6] A. V. Kabashin, P. Evans, S. Pastkovsky, W. Hendren, G. A. Wurtz, R. Atkinson, R. Pollard, V. A. Podolskiy, and A. V. Zayats, *Nat. Mater.* **8**, 867 (2009).
- [7] M. Navarro-Cía and S. A. Maier, *ACS Nano* **6**, 3537 (2012).
- [8] T. Shoji and Y. Tsuboi, *J. Phys. Chem. Lett.* **5**, 2957 (2014).
- [9] H. Aouani, M. Rahmani, M. Navarro-Cía, and S. A. Maier, *Nat. Nanotechnol.* **9**, 290 (2014).
- [10] R. Chikkaraddy, B. de Nijs, F. Benz, S. J. Barrow, O. A. Scherman, E. Rosta, A. Demetriadou, P. Fox, O. Hess, and J. J. Baumberg, *Nature (London)* **535**, 127 (2016).
- [11] F. Benz, M. K. Schmidt, A. Dreismann, R. Chikkaraddy, Y. Zhang, A. Demetriadou, C. Carnegie, H. Ohadi, B. de Nijs, R. Esteban, J. Aizpurua, and J. J. Baumberg, *Science* **354**, 726 (2016).
- [12] P. Vasa and C. Lienau, *ACS Photonics* **5**, 2 (2018).
- [13] A. Guerreiro, D. F. Santos, and J. M. Baptista, *Sensors* **19**, 1772 (2019).
- [14] D. F. Santos, A. Guerreiro, and J. M. Baptista, *IEEE Sensors J.* **17**, 2439 (2017).
- [15] B. Gallinet, J. Butet, and O. J. Martin, *Laser Photonics Rev.* **9**, 577 (2015).
- [16] R. Yu, L. M. Liz-Marzán, and F. J. García de Abajo, *Chem. Soc. Rev.* **46**, 6710 (2017).
- [17] F. J. García de Abajo, *J. Phys. Chem. C* **112**, 17983 (2008).
- [18] W. Zhu, R. Esteban, A. G. Borisov, J. J. Baumberg, P. Nordlander, H. J. Lezec, J. Aizpurua, and K. B. Crozier, *Nat. Commun.* **7**, 11495 (2016).
- [19] J. D. Cox and F. J. García de Abajo, *Nat. Commun.* **5**, 5725 (2014).
- [20] P. A. D. Gonçalves, T. Christensen, N. Rivera, A. P. Jauho, N. A. Mortensen, and M. Soljačić, *Nat. Commun.* **11**, 366 (2020).
- [21] J. M. Pitarke, V. M. Silkin, E. V. Chulkov, and P. M. Echenique, *Rep. Prog. Phys.* **70**, 1 (2007).
- [22] I. Ciraci, R. T. Hill, J. J. Mock, and Y. Urzhumov, A. I. Fernández-Domínguez, S. A. Maier, J. B. Pendry, A. Chilkoti, and D. R. Smith, *Science* **337**, 1072 (2012).
- [23] C. Ciraci, J. B. Pendry, and D. R. Smith, *ChemPhysChem* **14**, 1109 (2013).
- [24] M. Kupresak, X. Zheng, G. A. E. Vandenbosch, and V. V. Moshchalkov, *Adv. Theory Simul.* **1**, 1800076 (2018).
- [25] E. Madelung, *Naturwissenschaften (The Science of Nature)* **14**, 1004 (1926).
- [26] R. A. Alves, N. A. Silva, J. C. Costa, M. Gomes, and A. Guerreiro, in *Third International Conference on Applications of Optics and Photonics*, edited by M. F. P. C. M. Costa (SPIE, 2017), pp. 280–284.
- [27] L. Xu and H. Chen, *Nat. Photonics* **9**, 15 (2014).
- [28] A. Eguluz and J. J. Quinn, *Phys. Rev. B* **14**, 1347 (1976).
- [29] J. Zhang, J. B. Pendry, and Y. Luo, *Adv. Photonics* **1**, 014001 (2019).
- [30] V. Pacheco-Peña, A. I. Fernández-Domínguez, Y. Luo, M. Beruete, and M. Navarro-Cía, *Laser Photonics Rev.* **11**, 1700051 (2017).
- [31] A. Wiener, A. I. Fernández-Domínguez, A. P. Horsfield, J. B. Pendry, and S. A. Maier, *Nano Lett.* **12**, 3308 (2012).
- [32] E. Galiffi, J. B. Pendry, and P. A. Huidobro, *ACS Nano* **12**, 1006 (2018).
- [33] Y. Luo, A. Aubry, and J. B. Pendry, *Phys. Rev. B* **83**, 155422 (2011).
- [34] Y. Zeng, J. Liu, and D. H. Werner, *Opt. Express* **19**, 20035 (2011).

- [35] V. Pacheco-Peña, R. A. Alves, and M. Navarro-Cía, *ACS Photonics* **6**, 2014 (2019).
- [36] Y. Luo, J. B. Pendry, and A. Aubry, *Nano Lett.* **10**, 4186 (2010).
- [37] D. Y. Lei, A. Aubry, Y. Luo, S. A. Maier, and J. B. Pendry, *ACS Nano* **5**, 597 (2011).
- [38] V. Pacheco-Peña, M. Beruete, A. I. Fernández-Domínguez, Y. Luo, and M. Navarro-Cía, *ACS Photonics* **3**, 1223 (2016).
- [39] J. Kiusalaas, *Numerical Methods in Engineering with Python 3* (2013).